Single-molecule mechanics of mussel adhesion

Haeshin Lee*, Norbert F. Scherer†, and Phillip B. Messersmith*‡§

Departments of *Biomedical Engineering and ‡Materials Science and Engineering, Northwestern University, 2145 Sheridan Road, Evanston, IL 60208; and †Department of Chemistry and Institute for Biophysical Dynamics, University of Chicago, 5735 South Ellis Avenue, Chicago, IL 60637

Communicated by George C. Schatz, Northwestern University, Evanston, IL, July 3, 2006 (received for review April 5, 2006)

The glue proteins secreted by marine mussels bind strongly to virtually all inorganic and organic surfaces in aqueous environments in which most adhesives function poorly. Studies of these functionally unique proteins have revealed the presence of the unusual amino acid 3,4-dihydroxy-L-phenylalanine (dopa), which is formed by posttranslational modification of tyrosine. However, the detailed binding mechanisms of dopa remain unknown, and the chemical basis for mussels' ability to adhere to both inorganic and organic surfaces has never been fully explained. Herein, we report a single-molecule study of the substrate and oxidation-dependent adhesive properties of dopa. Atomic force microscopy (AFM) measurements of a single dopa residue contacting a wet metal oxide surface reveal a surprisingly high strength yet fully reversible, noncovalent interaction. The magnitude of the bond dissociation energy as well as the inability to observe this interaction with tyrosine suggests that dopa is critical to adhesion and that the binding mechanism is not hydrogen bond formation. Oxidation of dopa, as occurs during curing of the secreted mussel glue, dramatically reduces the strength of the interaction to metal oxide but results in high strength irreversible covalent bond formation to an organic surface. A new picture of the interfacial adhesive role of dopa emerges from these studies, in which dopa exploits a remarkable combination of high strength and chemical multifunctionality to accomplish adhesion to substrates of widely varying composition from organic to metallic.

3,4-dihydroxylphenylalanine | atomic force microscopy | mussel adhesive protein

Numerous living creatures rely on physical adhesion to biotic and abiotic objects for essential activities, such as movement, protection, and self-defense (1–3). From a purely functional point of view, bioadhesion can be of two major types: temporary and permanent. A characteristic example of a temporary bioadhesive strategy is given by the specialized foot hairs used by geckos for climbing sheer surfaces (1). A classic example of permanent bioadhesion is exemplified by mussels, (4) which secrete holdfasts essential for stability within the tidal marine environment. The remarkable features of mussel adhesion include the ability to achieve long-lasting adhesion in a wet environment (3) and adherence to virtually all types of inorganic and organic surfaces (5). The adhesive apparatus of the mussel consists of a series of byssal threads that tether the organism to a substrate (Fig. 1*A*). At least five specialized adhesive protein subtypes known to contain 3,4-dihydroxy-L-phenylalanine (dopa) at concentrations ranging from a few mol % to 27 mol % (Fig. 1*B*) are found within the distal adhesive pad of the widely studied blue mussel, *Mytilus edulis* (6). The highest dopa content occurs in *M. edulis* foot protein (Mefp)-3 (21 mol %) and Mefp-5 (27 mol %) (7, 8), both of which are localized near the interface between the adhesive pad and the substrate (Fig. 1*C*).

The role of dopa in mussel adhesive proteins is not fully understood, although there is general acceptance that oxidized dopa residues play important roles in cross-linking reactions leading to solidification of the secreted liquid protein adhesive (9–12). The particularly high concentration of dopa at the adhesive/substrate interface has led to much speculation regarding its role in adhesive bonding. However, the physicochemical details of dopa–surface interactions remain elusive. Byssal thread pull-off experiments (13) and macroscopic lap shear bond strength measurements using dopa-containing polypeptides (14) failed to clearly distinguish between cohesive and adhesive behavior and yielded little information at the molecular level. Previous atomic force microscopy (AFM) measurements of whole mussel adhesive proteins interacting with surfaces (15, 16) were complicated by the presence of other amino acids, an unknown number of proteins on the tip, and multiple dopa residues interacting with the surface. For this paper, we used the single-molecule method of Hinterdorfer *et al.* (17) to isolate the contribution of dopa in mussel adhesion.

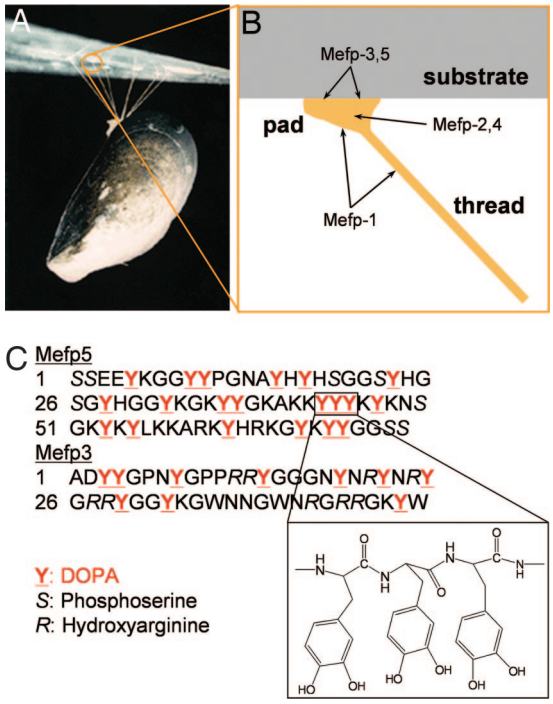

Fig. 1. Biodistribution and amino acid composition of mussel adhesive proteins of *M. edulis*. (*A*) Photograph of a mussel attached to a glass surface, showing the byssal threads and adhesive pads (33). (*B*) The biodistribution of Mefps. Mefp-3 and Mefp-5 are found at the pad–substrate interface. (*C*) The amino acid sequences of Mefp-3 and Mefp-5, which have the highest known dopa contents, at 21 and 27 mol %, respectively (7, 8). Also shown is the chemical structure of dopa as it appears in the tri-dopa sequence in residues 43–45 of Mefp-5.

Results and Discussion

Single-Molecule Adhesion Force of dopa. We used chemically modified Si_3N_4 AFM cantilevers to investigate the interaction of single dopa residues with organic and inorganic surfaces. PEG

Conflict of interest statement: No conflicts declared.

Abbreviations: AFM, atomic force microscopy; dopa, 3,4-dihydroxy-L-phenylalanine; Mefp, *Mytilus edulis* foot protein; F–D, force–distance.

§To whom correspondence should be addressed. E-mail: philm@northwestern.edu.

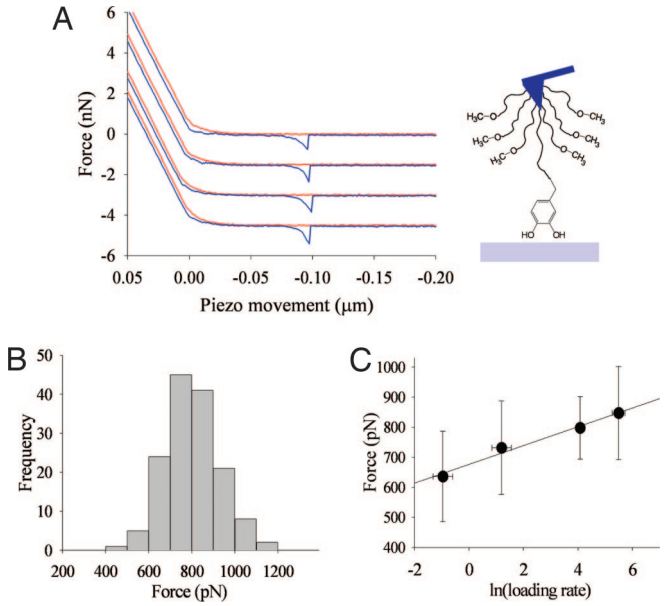

Fig. 2. dopa adheres strongly and reversibly to Ti surfaces. (*A*) Schematic of dopa-functionalized AFM tip and typical single-molecule F–D curves of dopa interacting with a Ti surface. The red and blue traces indicate approach and retraction signals, respectively, in which dopa–Ti adhesive (interaction) force was observed during retraction. The four different force curves were produced from the same dopa-functionalized tip and are displaced vertically for clarity. (*B*) Histogram ($n = 147$) of pull-off force values for dopa–Ti obtained with a single AFM tip at a loading rate of 60.0 nN/s. The mean force value was calculated to be 805 ± 131 pN. (*C*) A linear-log plot of force vs. loading rate for dopa–Ti. Mean forces and standard deviations obtained from a minimum of 30 adhesion events were 847 ± 157 pN (250.0 ± 62.0 nN/s), 805 ± 131 pN (60.0 ± 9.0 nN/s), 744 ± 207 pN (3.50 ± 1.5 nN/s), and 636 ± 151 (0.41 ± 0.15 nN/s).

was used as a linker and inert back-filling molecule to isolate the contribution of dopa (17). *N*-Boc-dopa was end-tethered to PEG, and the Boc protecting group remained in place to avoid electrostatic interactions. In a typical experiment, a dopa-functionalized AFM tip was lowered at a constant rate onto a wet surface to a maximum load of 15–20 nN and then retracted at the same rate while force versus extension was recorded. Force–distance (F–D) curves exhibit the characteristic point of separation of the tip from the surface and single-molecule adhesion events.

Fig. 2*A* shows representative F–D curves for approach and retraction of a dopa-modified cantilever from a Ti surface. The initial portion of the retraction curves exhibits an appearance typical of elastic extension of a tethered PEG chain (17), culminating in the detachment of dopa from the surface. Several features of the observed F–D curves are remarkable and provide convincing evidence for a high strength reversible single-molecule interaction. First, the essential features of the F–D curves were observed repeatedly during multiple pull-off experiments performed with the same tip, indicating that the interaction between dopa and the surface was both strong (≈800 pN) and reversible (i.e., could be repeatedly rebound and repulled). Second, the stretched contour length of PEG extrapolated from the F–D curves (36 nm) was consistent with the expected 37-nm contour length for the PEG molecular weight (3.4 kDa) used in this study. Third, inspection of data from multiple F–D curves revealed virtual overlap of the F–D traces and similar pull-off distances (Fig. 2*A*), suggesting that the same exact dopa–PEG chain was interacting with the Ti surface during successive tip contacts. Because of the high curvature of the cantilever tip (radius ≈ 25 nm) as well as the polydispersity of PEG, it would be unlikely to observe the same pull-off distances for dopa residues tethered to different PEG chains. On very rare occasions this did occur, which was apparent from F–D profiles that exhibited multiple pull-off signals (Fig. 5, which is published as supporting information on the PNAS web site). Finally, the low probability of observed tip–surface binding events (≈10% of contacts yielded F–D curves as shown in Fig. 2*A*) provided additional evidence for single dopa–Ti surface interactions.

The reversible nature of the interaction between a single dopa molecule and the Ti surface allowed us to construct a histogram of bond dissociation forces extracted from many F–D curves (Fig. 2*B*), yielding a surprisingly large dissociation force of 805 ± 131 pN (147 events, 3 cantilevers) for the mean and standard deviation. To put this value in perspective, other investigators have determined that a few nanonewtons of applied force was required to rupture a single covalent bond (18). Obviously, once covalent bonds have ruptured, one cannot study reversible binding dynamics of single molecules but must average over the behavior of many single molecules. On the other hand, hydrogen bonds, although reversible, ruptured at tens of piconewton forces (19). To our knowledge, the dopa–Ti interaction is the strongest reversible binding interaction involving a small biological molecule ever reported, underscoring the unique nature of the observed dopa–Ti interaction.

In the absence of dopa, PEG-functionalized AFM tips showed essentially no hysteresis between approach and pull-off curves in experiments conducted under identical conditions (Fig. 6, which is published as supporting information on the PNAS web site), indicating that the PEG itself interacts very weakly with the Ti substrate. Furthermore, when *N*-Boc-protected tyrosine (*N*-Boc-Tyr) was substituted for dopa, only small-amplitude interaction forces (97 ± 28 pN) (Fig. 7, which is published as supporting information on the PNAS web site) were measured to Ti. This small interaction clearly demonstrates the significance of Tyr-to-dopa posttranslational modification in the adhesion of mussel adhesive proteins.

To gain further insight into the energetics of this interaction we determined the average dopa–Ti bond rupture force at several loading rates. The plot of force vs. loading rate is shown in Fig. 2*C*, revealing the expected trend of increased force to break the bond at higher loading rates (20). The linear fit to the data provides the bond dissociation energy and the distance (x_b) beyond which the bond is completely dissociated along the applied force direction (20, 21). The analysis revealed a dissociation energy of 22.2 kcal/mol and an x_b value of 2.16 Å for the dopa–Ti bond. The determined bond dissociation energy is close to the 25–30 kcal/mol range estimated by density functional theory for the bond formed between dopamine and TiO_2 (22). Although the existence of metal–oxygen coordination is well established in biology, the metal–oxygen coordination bond formed by interaction of dopa with an oxide surface is a rare example of a coordination bond whose primary function is to achieve mechanical adhesion. Although the interaction is reversible in our single-molecule experiments, it may not be the case for whole mussel adhesive proteins, because cooperativity of multiple dopa–surface interactions could allow for enormous force transmission across the interface. As few as three or four dopa residues interacting with an oxide surface would eclipse the strength of a covalent bond, leading to irreversible cohesive failure (i.e., covalent bond breakage) within the bulk adhesive pad. This may help to explain previous observations that Mefp-3 and Mefp-5 proteins remain attached to surfaces after removal of the adhesive pad (23).

Effect of dopa Oxidation on Adhesion. Oxidation of the catechol side chain of dopa occurs in the alkaline marine environment, giving rise to quinones that further react to cross-link adhesive proteins via aryl–aryl coupling (di-dopa formation) or possibly via Michael-type addition reactions with amine-containing pro-

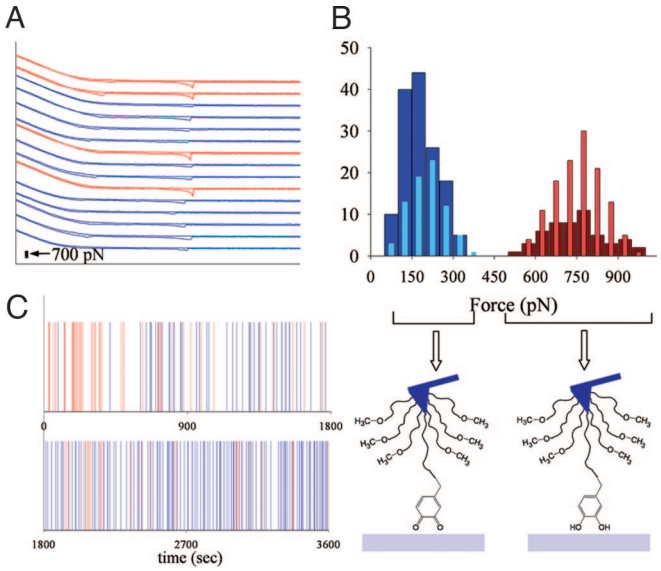

Fig. 3. Oxidation of dopa reduces adhesion to Ti surfaces. (*A*) Bimodal force signals from dopa contacting Ti under alkaline conditions (pH 9.7). Selected AFM F–D scans obtained during a 1-h experiment under alkaline conditions (20 mM Tris·HCl, pH 9.7) are shown, with time increasing from the top of the graph to the bottom (top, $t = 0$; bottom, $t = 1$ h; 1,800 repetitions total). Detectable force signals were found in ≈10% of the F–D curves obtained. F–D curves exhibiting strong dopa–Ti interactions are shown in red, whereas F–D curves shown in blue exhibited much weaker interactions. The weak force signals appeared only under alkaline conditions and were not observed at neutral pH. (*B*) Structure-based assignments of the adhesive molecules dopa and dopa–quinone by analysis of 1,800 F–D curves each from two pH conditions (pH 9.7 and 8.3). Bimodal force distributions were measured with averages in a low-force regime [180 ± 60 pN (145 events, pH 9.7) and 206 ± 66 pN (76 events, pH 8.3)] or in a high-force regime [740 ± 110 pN (51 events, pH 9.7) and 759 ± 88 pN (126 events, pH 8.3)]. Considering the pK_a (9.2) of the dopa hydroxyl group, the dopa structure is favored over dopa–quinone at low pH, resulting in more frequent detection of high bond force and vice versa at high pH. Considering also the results shown in Fig. 2, which were obtained under a neutral pH condition, where no low-force regime was detected, the strong adhesive interactions are assigned to unoxidized dopa–Ti interaction, whereas the weak adhesive interactions are assigned to the dopa–quinone–Ti interaction. (*C*) Time trajectory display of the force signals of dopa (red) and dopa–quinone (blue) at pH 9.7 (the time trajectory display at pH 8.3 is available in Fig. 8, which is published as supporting information on the PNAS web site).

tein residues (9–12). The prevailing view is that these reactions play key roles in the bulk solidification of mussel glues; however, very little is known about the impact of these oxidation reactions on adhesion to substrates (14). Measurement of adhesive interactions between oxidized dopa and surfaces is complicated by the highly reactive nature of semiquinones and quinones. This technical concern was alleviated through the use of a large excess of unreactive methoxy-PEG during tip functionalization, yielding a single dopa molecule on the AFM tip. The excess methoxy-PEG molecules suppressed possible intermolecular reactions between oxidized dopa species and allowed us to investigate adhesive interactions between oxidized dopa and various surfaces in great detail.

An AFM tip containing a single dopa residue was first identified by obtaining F–D curves on Ti at neutral pH as described above. The pH of the aqueous solution was then increased to 8.3 or 9.7 to oxidize the dopa, after which additional F–D curves were recorded. Interestingly, at alkaline pH values, a bimodal distribution of force signals is observed consisting of large or small forces registered at similar pull-off distances (Fig. 3*A*). Statistical analysis of the pH 9.7 data yielded two nonoverlapping histograms with force values of 180 ± 60 pN (74% frequency) and 740 ± 110 pN (26% frequency) (Fig. 3*B*, dark blue bars and dark red bars, respectively). Similar force values were obtained at pH 8.3, except that the likelihood of observing a force value in the range ≈750–800 pN increased to 62%, whereas the likelihood of observing a force value in the 150- to 200-pN range decreased to 38% (Fig. 3*B*, light red bars and light blue bars, respectively). These observations are consistent with the observation of single-molecule fluctuations between two states in chemical equilibrium; i.e., between dopa and dopa–quinone (Fig. 3*C*). The equilibrium between dopa and dopa–quinone is shifted toward dopa–quinone at high pH ($pK_a = 9.2$) (24). Considering the data in Fig. 3 as well as the neutral pH data shown in Fig. 2, we assign the high-force signal to the interaction of dopa with Ti and deduce that the low-force signal represents the interaction of dopa–quinone and its resonance structures with Ti, because these signals appeared only under oxidizing conditions. Assuming a value for the bond length, x_b, similar to that observed for dopa–Ti (2.1 Å), the calculated bond dissociation energy of dopa–quinone to Ti was only 5.3 kcal/mol (≈8.5 kT) (details are in *Supporting Text*, which is published as supporting information on the PNAS web site), confirming that oxidation of dopa substantially reduces adhesion to Ti. It is, therefore, unlikely that mussel adhesion to wet Ti or similar oxide surfaces is mediated by dopa–quinone and its resonance structures.

Adhesion Mechanism of dopa on Organic Surfaces. Finally, we used a similar methodology to elucidate the mechanism behind mussel adhesion to organic surfaces. In contrast to inorganic surfaces, we anticipated that oxidation of dopa under elevated pH may result in covalent coupling to organic surfaces. It has been speculated that reactions between dopa–quinone and either primary amines (10) or thiols (25), for example, give rise to bulk cohesive cross-linking of marine adhesive proteins. However, clear evidence for such reactions occurring at interfaces has been lacking.

Interfacial reactions between oxidized dopa and organic surfaces were probed in three steps. First, the characteristic single-molecule dopa–Ti interaction was identified through F–D curves obtained at neutral pH as described above. The Ti surface was then replaced with an amine-modified Si surface (Fig. 9, which is published as supporting information on the PNAS web site) (26) and force experiments with the same tip were performed at pH 9.7. Initial F–D curves showed no significant hysteresis, however within a short period (156 seconds; 78th contact/pull-off cycle) a dramatic increase in pull-off force to 2.2 nN is observed, after which an additional 800 contact/pull-off cycles revealed no measured interaction force (Fig. 4*A*). The extremely large force value together with the lack of subsequent adhesion events is consistent with covalent bond rupture, leading us to conclude that dopa–nitrogen adducts form under the conditions of our experiment (Fig. 4*B*). We do not know where covalent bond breakage occurs, however the magnitude of the rupture force is consistent with rupture of a silicon–carbon bond (2.0 ± 0.3 nN) (18), suggesting that the broken covalent bond may be at the organic–inorganic interface of the Si_3N_4 tip. Although the pH used in our experiments is somewhat higher than that of seawater, we believe that the results will be essentially similar at lower pH values, albeit with slower kinetics because of the shift in chemical equilibria of dopa–quinone/dopa and NH_2/NH_3^+ toward dopa and NH_3^+ species, respectively.

The overall picture of mussel adhesion that emerges from our findings is one of unique chemical versatility that permits strong adhesion to both organic and inorganic surfaces. The conversion of tyrosine to dopa is a crucial event in mussel adhesive protein processing that leads to multiple adhesive

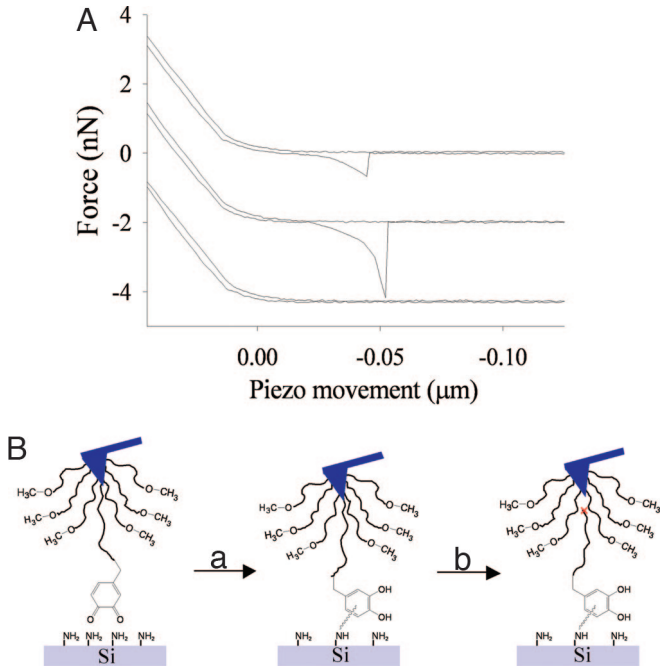

Fig. 4. Oxidation of dopa increases adhesion to organic surfaces. (*A*) Selected F–D curves for interaction of a dopa-modified AFM tip with an organic surface. First, the presence of dopa was confirmed by obtaining a F–D curve at neutral pH on Ti (top curve), showing the expected pull-off force of ≈800 pN. Next, the same tip was allowed to interact with an amine presenting organic surface (*Supporting Text*) at pH = 9.7, upon which a pull-off force of 2.2 nN was observed (middle curve). The magnitude of the pull-off force is consistent with covalent bond rupture, and subsequent F–D curves (n = 800) failed to show a detectable interaction force (bottom curve). (*B*) Schematic illustration of covalent bond formation between dopa and amines at the organic surface. The high-magnitude pull-off force, along with lack of subsequent observations of tip–molecule–surface interaction events, suggests that dopa–quinone formed a covalent bond to surface-bound amine, possibly via a Michael addition-type of reaction (10–13). The location of the ruptured covalent bond is not known; although, under the conditions of this experiment, it is not expected to re-form, explaining the absence of an adhesion event in subsequent F–D curves.

roles for dopa at interfaces. On inorganic surfaces the unoxidized dopa forms high-strength yet reversible coordination bonds, whereas on organic surfaces oxidized dopa is capable of adhering via covalent bond formation. It may be that the remarkable ability of mussels to adhere to both organic and inorganic surfaces is related in part to the equilibrium that exists between dopa and dopa–quinone at marine pH, allowing both species to interact with surfaces. It is also notable that strong bonds between dopa and organic and inorganic surfaces formed in the presence of water, presumably a crucial characteristic for a protein adhesive operating in the wet marine environment. As our understanding of mussel adhesion expands, so do the prospects for exploiting this information for practical use. Indeed, the use of dopa and related catecholic molecules has recently emerged as a promising method for anchoring synthetic and biological macromolecules onto oxide surfaces for medical applications (27–29).

Methods

Tip Modification. Before surface modification, silicon nitride (Si_3N_4) tips were cleaned in an O_2 plasma (Harrick Scientific, Ossining, NY) for 3 min and then subsequently transferred to a piranha solution (sulfuric acid/H_2O_2, 8:2) for 30 min. After extensive rinsing with nanopure H_2O, the tips were transferred into 20% (vol/vol) 3-aminopropyltrimethoxysilane in toluene for 30–60 min, resulting in an aminosilane-functionalized tip. The aminated AFM tips were then functionalized with a mixture of methoxy-PEG-*N*-hydroxy succinimide (mPEG-*N*HS; Nektar, Huntsville, AL), which had a molecular weight of 2,000, and Fmoc-PEG-*N*-hydroxy succinimide (Fmoc-PEG-*N*HS; Nektar), which had a molecular weight of 3,400, at a Fmoc-PEG-*N*HS/mPEG-*N*HS ratio of 1:5 to 1:10. The PEG functionalization was performed at a total PEG concentration of 5 mM in 50 mM sodium phosphate buffer/0.6 M K_2SO_4, pH 7.8, at 40°C and subsequently repeated in chloroform at room temperature for 3 h. Fmoc protecting groups were then cleaved by treating the tips in 20% piperidine (vol/vol in *N*-methyl-2-pyrrolidone) for 5 min, followed by coupling of *N*-Boc-dopa to the liberated amine in solution with 10 μl of diisopropylethylamine [*N*-nitrosobis(2-oxopropyl)amine/hydroxybenzotriazole/dopa molar ratio of 1:1:1; 8 mM in *N*-methyl-2-pyrrolidone]. The use of excess mPEG-*N*HS during PEG functionalization of the tip served to limit the number of dopa residues on the tip, facilitating single-molecule force measurements. The same procedure was used for preparation of Boc-tyrosine-functionalized tips.

Surface Preparation and Characterization. A 20- to 50-nm (thin) layer of Ti on Si [crystal structure of (100)] wafer surfaces was prepared with an Edwards FL400 e-beam evaporator (Boc Edwards, Sussex, U.K.). Before use, all surfaces were sonicated (model no. 3214 sonicator; Branson, Dansbury, CT) in hexane, 2-propanol, and acetone and, subsequently, in piranha solution to generate an oxide layer. Amine-containing organic surfaces were prepared by functionalization of unmodified silicon wafers with 3-aminopropyltrimethoxysilane in anhydrous toluene after the cleaning process just described. The presence of surface amines was confirmed by x-ray photoelectron spectroscopy (Fig. 9). Unmodified and 3-aminopropyltrimethoxysilane-modified Si surfaces were analyzed by x-ray photoelectron microscopy, (Omicron, Taunusstein, Germany) equipped with a monochromatic Al Kα (1,486.8 eV), 300-W x-ray source and an electron gun to eliminate charge build-up. The iron-oxide surface was prepared by chemical vapor deposition through the reaction of iron chloride with water at a temperature range of 800–1,000°C (30).

AFM Experiment. All data were collected on an Asylum MFP-1D AFM instrument (Asylum Research, Santa Barbara, CA). Spring constants of individual cantilevers (Veeco Probes, Santa Barbara, CA, and Bio-Levers; Olympus, Tokyo, Japan) were calibrated by applying the equipartition theorem to the thermal noise spectrum (31). All AFM experiments were conducted in Millipore (Billerica, MA) water or water buffered with 20 mM Tris·HCl (pH 9.7 and 8.3) at room temperature. The progress of tip functionalization with 3-aminopropyltrimethoxysilane and PEG was confirmed by the appearance of characteristic force signals at each step in the modification procedure (Fig. 6). The vast majority of dopa-functionalized AFM tips yielded F–D curves with only a single dopa adhesion event, although, on one occasion, a tip generated two spatially resolved adhesion events during pull-off (Fig. 5). Control experiments performed with AFM tips modified as described above with Boc-tyrosine revealed only weak interactions with Ti surfaces (Fig. 7*A*). The presence of tyrosine was confirmed by force measurements on gold-evaporated surfaces (Fig. 7*B*).

Dynamic Force Experiments. AFM experiments were performed as described above at several loading rates. The actual loading rate was directly determined from each individual force–extension curve as follows. Four data points were taken near the rupture point and plotted as a function of time as determined from the AFM piezo-transducer ramp rate. The slope ($\Delta F/\Delta t$ in nN/sec) was calculated by a linear least-square fit of the plots (32).

We thank Dr. Jason Ming Zhao for technical support and insightful discussions; Northwestern University for use of its Atomic and Nanoscale

Characterization Experimental Center; and the National Science Foundation for use of its Materials Research Science and Engineering Centers facilities, which are supported by the University of Chicago through Grant DMR 0213745. This work was supported by National Institutes of Health Grant DE 14193, Biologically Inspired Materials Program Grant NCC-1-02037 from the University Research Technology Institute of the National Aeronautics and Space Administration, and a seed grant from the University of Chicago's Institute for Biophysical Dynamics.

1. Autumn, K., Liang, Y. A., Hsieh, S. T., Zesch, W., Chan, W. P., Kenny, T. W., Fearing, R. & Full, R. J. (2000) *Nature* **405,** 681–685.
2. Chisholm, J. R. M. & Kelley, R. (2001) *Nature* **409,** 152.
3. Waite, J. H. (2002) *Integr. Comp. Biol.* **42,** 1172–1180.
4. Waite, J. H. & Tanzer, M. L. (1981) *Science* **212,** 1038–1040.
5. Crisp, D. J., Walker, G., Young, G. A. & Yule, A. B. (1985) *J. Colloid Interface Sci.* **104,** 40–50.
6. Waite, J. H. (1999) *Ann. N.Y. Acad. Sci.* **875,** 301–309.
7. Papov, V. V., Diamond, T. V., Biemann, K. & Waite, J. H. (1995) *J. Biol. Chem.* **270,** 20183–20192.
8. Waite, J. H. & Qin, X. (2001) *Biochemistry* **40,** 2887–2893.
9. Yu, M., Hwang, J. & Deming, T. J. (1999) *J. Am. Chem. Soc.* **121,** 5825–5826.
10. Burzio, L. A. & Waite, J. H. (2000) *Biochemistry* **39,** 11147–11153.
11. Haemers, S., Koper, G. J. M. & Frens, G. (2003) *Biomacromolecules* **4,** 632–640.
12. Monahan, J. & Wilker, J. J. (2004) *Langmuir* **20,** 3724–3729.
13. Young, G. A. & Crisp, D. J. (1982) in *Adhesion*, ed. Allen, K. W. (Applied Science, London), pp. 19–39.
14. Yu, M. & Deming, T. J. (1998) *Macromolecules* **31,** 4739–4745.
15. Frank, B. P. & Belfort, G. (2002) *Biotech. Prog.* **18,** 580–586.
16. Hwang, D. S., Yoo, H. J., Jun, J. H., Moon, W. K. & Cha, H. J. (2004) *Appl. Environ. Microbiol.* **70,** 3352–3359.
17. Hinterdorfer, P., Baumgartner, W., Gruber, H. J., Schilcher, K. & Schindler, H. (1996) *Proc. Natl. Acad. Sci. USA* **93,** 3477–3481.
18. Oesterhelt, F., Rief, M. & Gaub, H. E. (1999) *N. J. Phys.* **1,** 1–11.
19. Grandbois, M., Beyer, M., Rief, M., Clausen-Schaumann, H. & Gaub, H. E. (1999) *Science* **283,** 1727–1730.
20. Liphardt, J., Onoa, B., Smith, S. B., Tinacio, J. I. & Bustamante, C. (2001) *Science* **292,** 733–737.
21. Merkel, R., Nassoy, P., Leung, A., Ritchie, K. & Evans, E. (1999) *Nature* **397,** 50–53.
22. Vega-Arroyo, M., LeBreton, P. R., Rajh, T., Zapol, P. & Curtiss, L. A. (2005) *Chem. Phys. Lett.* **406,** 306–311.
23. Zhao, H., Robertson, N. B., Jewhurst, S. A. & Waite, J. H. (2006) *J. Biol. Chem.* **281,** 11090–11096.
24. Rodriguez, R., Blesa, M. A. & Regazzoni, A. E. (1996) *J. Colloid Interface Sci.* **177,** 122–131.
25. Zhao, H., Sun, C., Stewart, R. J. & Waite, J. H. (2005) *J. Biol. Chem.* **280,** 42938–42944.
26. Fadeev, A. Y. & McCarthy, T. J. (2000) *Langmuir* **16,** 7268–7274.
27. Paunesku, T., Rajh, T., Wiederrecht, G., Maser, J., Vogt, S., Stojicevic, M., Protic, M., Lai, B., Oryhon, J., Thurnauer, M. & Woloschak, G. (2003) *Nat. Mat.* **2,** 343–346.
28. Statz, A. R., Meagher, R. J., Barron, A. E. & Messersmith, P. B. (2005) *J. Am. Chem. Soc.* **127,** 7972–7973.
29. Dalsin, D. L., Hu, B.-H., Lee, B. P. & Messersmith, P. B. (2003) *J. Am. Chem. Soc.* **125,** 4253–4258.
30. Pierson, H. O. (1992) *Handbook of Chemical Vapor Deposition* (Noyes, Park Ridge, NJ).
31. Hutter, J. L. & Bechhoefer, J. (1993) *Rev. Sci. Instr.* **64,** 1868–1873.
32. Leckband, D. & Israelachvili, J. (2001) *Q. Rev. Biophys.* **2,** 105–267.
33. Waite, J. H. (1991) *Chem. Ind. (London)* **17,** 607.